

A new dataset of river flood hazard maps for Europe and the Mediterranean Basin

Francesco Dottori¹, Lorenzo Alfieri², Alessandra Bianchi³, Jon Skoien¹, Peter Salamon¹

1: European Commission, Joint Research Centre, Via E. Fermi 2749, 21027 Ispra, Italy.

2: CIMA Research Foundation, Savona, Italy

3: FINCONS SPA, Italy

Correspondence to: francesco.dottori@ec.europa.eu

Keywords: river flooding, flood hazard mapping, Europe, EFAS, Mediterranean Basin.

Abstract

In recent years, the importance of continental-scale hazard maps for riverine floods has grown. Nowadays, such maps are used for a variety of research and commercial activities, such as evaluating present and future risk scenarios and adaptation strategies, as well as supporting national and local flood risk management plans. In this paper we present a new set of high-resolution (100 metres) hazard maps for river flooding that covers most European countries, as well as all of the river basins entering the Mediterranean and Black Seas in the Caucasus, Middle East and Northern Africa countries. The new river flood hazard maps represent inundation along 329,000 km of the river network, for six different flood return periods, expanding on the datasets previously available for the region. The input river flow data for the new maps are produced by means of the hydrological model LISFLOOD using new calibration and meteorological data, while inundation simulations are performed with the hydrodynamic model LISFLOOD-FP. In addition, we present here a detailed validation exercise using official hazard maps for Hungary, Italy, Norway, Spain and the UK, which provides a more detailed evaluation of the new dataset compared with previous works in the region. We find that the modelled maps can identify on average two-thirds of reference flood extent, but they also overestimate flood-prone areas for flood probabilities below 1-in-100 years, while for return periods equal to or above 500 years the

29 maps can correctly identify more than half of flooded areas. Further verification is required in
30 North African and Eastern Mediterranean regions, in order to understand better the performance
31 of the flood maps in arid areas outside Europe. We attribute the observed skill to a number of
32 shortcomings of the modelling framework, such as the absence of flood protections and rivers
33 with upstream area below 500 km², and the limitations in representing river channels and
34 topography of lowland areas. In addition, the different designs of reference maps (e.g. extent of
35 areas included) affects the correct identification of the areas for the validation, thus penalizing the
36 scores. However, modelled maps achieve comparable results to existing large-scale flood models
37 when using similar parameters for the validation. We conclude that recently released high-
38 resolution elevation datasets, combined with reliable data of river channel geometry, may greatly
39 contribute to improving future versions of continental-scale river flood hazard maps. The new
40 high-resolution database of river flood hazard maps is available for download at
41 <http://data.europa.eu/89h/1d128b6c-a4ee-4858-9e34-6210707f3c81> (Dottori et al., 2020a).

42

43 *1) Introduction*

44 Nowadays, flood hazard maps are a basic requirement of any flood risk management strategy (EC
45 2007). Such maps provide spatial information about a number of variables (e.g. flood extent,
46 water depth, flow velocity) that are crucial to quantify flood impacts and therefore to evaluate
47 flood risk. Moreover, they can be used as a powerful communication tool, enabling the quick
48 visualization of the potential spatial impact of a river flood over an area.

49 In recent years, continental- and global-scale flood maps have grown in importance, and these
50 maps are now used for a variety of research, humanitarian and commercial activities, and as a
51 support of national and local flood management (Ward et al., 2015; Trigg et al., 2016). Global
52 flood maps are used to provide flood risk information and to support decision-making in spatial
53 and infrastructure planning, in countries where national level assessments are not available (Ward
54 et al., 2015). Moreover, continental and global hazard maps are vital for consistent quantification
55 of flood risk and for projecting the impacts of climate change (Alfieri et al., 2015; Trigg et al.,
56 2016; Dottori et al., 2018), thereby allowing for comparisons between different regions, countries
57 and river basins (Alfieri et al., 2016). Quantitative and comparable flood risk assessments are also
58 necessary to derive measurable indicators of the targets set by international agreements such as
59 the Sendai Framework for Disaster Risk Reduction (UNISDR, 2015).

60 In Europe, continental-scale flood hazard maps have been produced by Barredo et al. (2007),
61 Feyen et al. (2012), Alfieri et al. (2014), Dottori et al. (2016a) and Paprotny et al. (2017). These
62 maps have been used for a variety of studies, such as the evaluation of river flood risk under future
63 socio-economic and climate scenarios (Barredo et al., 2007; Feyen et al., 2012; Alfieri et al.,
64 2015), the evaluation of flood adaptation measures (Alfieri et al., 2016) and near real-time rapid
65 risk assessment (Dottori et al., 2017).

66 The quality of continental-scale flood maps is constantly improving, thanks to the increasing
67 accuracy of datasets and modelling tools. Wing et al., (2017) developed a dataset of flood hazard
68 maps for the conterminous United States using detailed national datasets and high-resolution
69 hydrodynamic modelling, and demonstrated that continental-scale maps can achieve an accuracy
70 similar to official national hazard maps, including maps based on accurate local-scale studies.
71 Moreover, Wing et al. used the same official hazard maps to evaluate the performance of the
72 global flood hazard model developed by Sampson et al. (2015). While the global model was less
73 accurate than the continental version, it was able to identify correctly over two-thirds of flood

74 extent. Conversely, European-scale maps have undergone limited testing against official hazard
75 maps, due to limitations in accessing official data (Alfieri et al., 2014).
76 Here, we present a new set of flood hazard maps at 100 metres resolution (Dottori et al., 2020a),
77 developed as a component of the Copernicus European Flood Awareness System (EFAS,
78 www.efas.eu). The new dataset builds upon the map catalogue developed by Dottori et al (2016a),
79 and features several improvements. The geographical extent of the new maps has been expanded
80 to include all geographical Europe (with the exclusion of the Volga river basin), the rivers entering
81 the Mediterranean Sea and the Black Sea (with the partial inclusion of the Nile river basin), plus
82 Turkey, Syria and the Caucasus region. To the best of our knowledge, these are the first flood
83 hazard maps available at 100 metres resolution for the whole region of the Mediterranean Basin.
84 The hydrological input data are calculated using the LISFLOOD hydrological model (van der
85 Knijff et al., 2010; Burek et al, 2013; <https://ec-jrc.github.io/lisflood/>), based on updated routines
86 and input data in respect to the previous dataset by Dottori et al. (2016a). Flood simulations are
87 performed with the hydrodynamic model LISFLOOD-FP (Bates et al., 2010; Shaw et al., 2021),
88 following the approach developed by Alfieri et al., (2014; 2015).
89 To provide a comprehensive overview of the skill of the new hazard maps, we perform a
90 validation exercise using official hazard maps for a number of countries, regions and large river
91 basins in Europe. The number and extent of the validation sites allows for a more detailed
92 evaluation with respect to previous efforts by Alfieri et al. (2014) and Paprotny et al. (2017), even
93 though none of the validation sites is located outside Europe (due the unavailability of national
94 flood maps). Finally, we discuss the results of the validation in light of previous literature studies,
95 we compare the performance of the present and previous versions of the flood hazard map dataset,
96 and we discuss a number of tests with alternative datasets and methods.

97 *2) Data and methods*

98 In this Section we describe the procedure adopted to produce and validate the flood hazard maps.
99 The hydrological input data consist of daily river flow for the years 1990-2016, produced with
100 the hydrological model LISFLOOD (see Section 2.1), based on interpolated daily meteorological
101 observations. River flow data are analysed to derive frequency distributions, peak discharges and
102 flood hydrographs, as described in Section 2.2. Flood hydrographs are then used to simulate
103 flooding processes at local scale with the LISFLOOD-FP hydrodynamic model (Section 2.3).

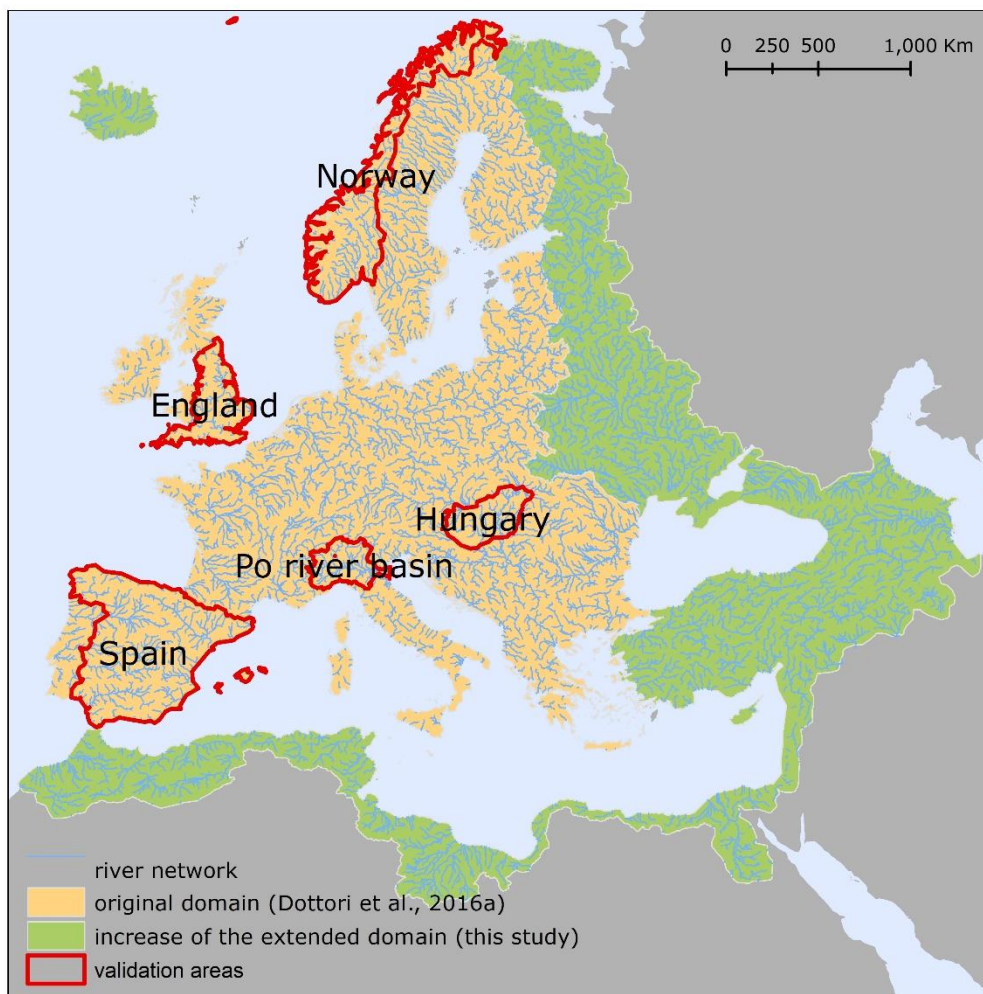
104 Finally, Section 2.4 describes the validation exercise and the comparison of different approaches
105 and input datasets.

106 *2.1 The LISFLOOD model*

107 LISFLOOD (Burek et al, 2013; van der Knijff et al., 2010) is a distributed, physically-based
108 rainfall-runoff model combined with a routing module for river channels. For this work we used
109 an updated version of LISFLOOD, released as open-source software and available at [https://ec-](https://ec-jrc.github.io/lisflood/)
110 [jrc.github.io/lisflood/](https://ec-jrc.github.io/lisflood/). The new version features an improved routine to calculate water
111 infiltration, the possibility of simulating open water evaporation and minor adjustments that
112 correct previous code inconsistencies (Arnal et al., 2019). The model is applied to run a long-term
113 hydrological simulation for the period 1990-2016 at 5 km grid spacing and at daily resolution,
114 which provides the hydrological input data for the flood simulations. Note that the same
115 simulation also provides initial conditions for daily flood forecast issued by EFAS.

116 The long-term run of LISFLOOD is driven by gridded meteorological maps, derived by
117 interpolating meteorological observations from stations and precipitation datasets (see Appendix
118 A for details). The meteorological dataset has been updated with respect to the dataset used by
119 Dottori et al. (2016a), to include new stations and gridded datasets across the new EFAS domain
120 (Arnal et al. 2019). In addition, LISFLOOD simulations require a number of static input maps
121 such as land cover, digital elevation model (DEM), drainage network, soil parameters and
122 parameterization of reservoirs. All the static maps have been updated to cover the whole EFAS
123 domain depicted in Figure 1. Further details on the static maps are provided by Arnal et al. (2019).
124 The current LISFLOOD version also benefits from an updated calibration at European scale,
125 based on the Evolutionary Algorithm approach (Hirpa et al., 2018) with the modified Kling-Gupta
126 efficiency criteria (KGE; Gupta et al., 2009) as objective function, and streamflow data for 1990-
127 2016 from more than 700 gauge stations. The same stations have been used to validate model
128 results, considering different periods of the time-series. The calibration and validation procedure
129 and the resulting hydrological skill are described by Arnal et al (2019), and summarized in
130 Appendix B. While we did not carry out a formal comparison with the previous LISFLOOD
131 calibration, which used a different algorithm and performance indicators (Zajac et al., 2013), the
132 larger dataset of streamflow observations and the improvement of the calibration routines should
133 provide a better performance.

134 The geographical extent used in the present study to produce the flood maps follows the recent
135 enlargement of EFAS (Arnal et al., 2019), and is shown in Figure 1. The new domain is
136 approximately 8,930,000 km² wide (an increase of 76% compared with the previous extent). The
137 new extent covers the entire area of geographical Europe (with the exclusion of the Volga river
138 basin and a number of river basins of the Arctic Sea in Russia), all the rivers entering the
139 Mediterranean and Black Seas (with a partial inclusion of the Nile river basin), plus the entire
140 territories of Armenia, Georgia, Turkey, and most of Syria and Azerbaijan. The river network
141 included in the new flood hazard maps has a total length of 329,000 km, with an 80% increase
142 compared with the previous flood maps (Alfieri et al., 2015; Dottori et al., 2016a).



143
144 *Figure 1. Geographical extent of the EFAS extended domain covered by the present dataset of*
145 *flood hazard maps. The extent of the map dataset produced by Dottori et al. (2016a) is depicted*
146 *in beige, while the regions added with the extended domain are in green. The Figure also displays*

147 *the river network considered by the flood maps and the areas used for the validation exercise (see*
148 *Sections 2.3 and 3).*

149 **2.2 Hydrological input of flood simulations**

150 The hydrological input data required for the flood simulations are provided using synthetic flood
151 hydrographs, following the approach proposed by Alfieri et al. (2014).

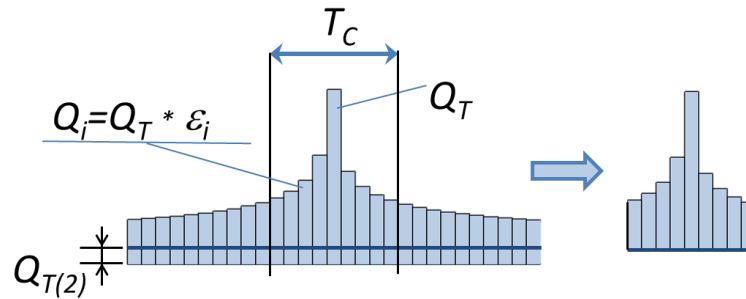
152 We use the streamflow dataset derived from the long-term run of LISFLOOD described in Section
153 2.1, considering the rivers with upstream drainage areas larger than 500 km². This threshold was
154 selected because the meteorological input data cannot accurately capture the short and intense
155 rainfall storms that induce extreme floods in small river basins, and therefore the streamflow
156 dataset does not represent accurately the flood statistics of smaller catchments (Alfieri et al.,
157 2014).

158 For each pixel of the river network we selected annual maxima over the period 1990-2016 and
159 we used the L-moments approach to fit a Gumbel distribution and calculate peak flow values for
160 reference return periods of 10, 20, 50, 100, 200 and 500 years. We also calculated the 30- and
161 1,000-year return periods in limited parts of the model domain to allow validation against official
162 hazard maps, see Section 2.3. We used the Gumbel distribution to keep a parsimonious
163 parameterization (two parameters instead of three for the generalized extreme value (GEV), log-
164 normal and other distributions), thus avoiding over-parameterization when extracting high return
165 period maps from a relatively short time-series. The same distribution was also adopted for the
166 extreme value analysis in previous studies regarding flood frequency and hazard (Alfieri et al.,
167 2014, 2015; Dottori et al., 2016).

168 Subsequently, we calculate a Flow Duration Curve (FDC) from the streamflow dataset. The FDC
169 is obtained by sorting in decreasing order all the daily discharges, thus providing annual
170 maximum values Q_D for any duration i between 1 and 365 days. Annual maximum values are
171 then averaged over the entire period of data, and used to calculate the ratios ε_i between each
172 average maximum discharge for i -th duration $Q_{D(i)}$ and the average annual peak flow (i.e. $Q_D = 1$
173 day). Such a procedure was carried out for all the pixels of the river network.

174 The synthetic flood hydrographs are derived using daily time-steps. The peak value of the
175 hydrograph is given by the peak discharge for the selected T -year return period Q_T , while the
176 other values for Q_i are derived by multiplying Q_T by the ratio ε_i . The hydrograph peak Q_T is placed

177 in the centre of the hydrograph, while the other values for Q_i are sorted alternatively to produce a
 178 triangular hydrograph shape, as shown in Figure 2. The total duration of the synthetic hydrograph
 179 is given by the local value of the time of concentration T_c , such that all of the durations $> T_c$ are
 180 discarded from the final hydrograph (Figure 2).



181

182 *Figure 2. General scheme of flood hydrographs (adapted from Alfieri et al., 2014).*

183

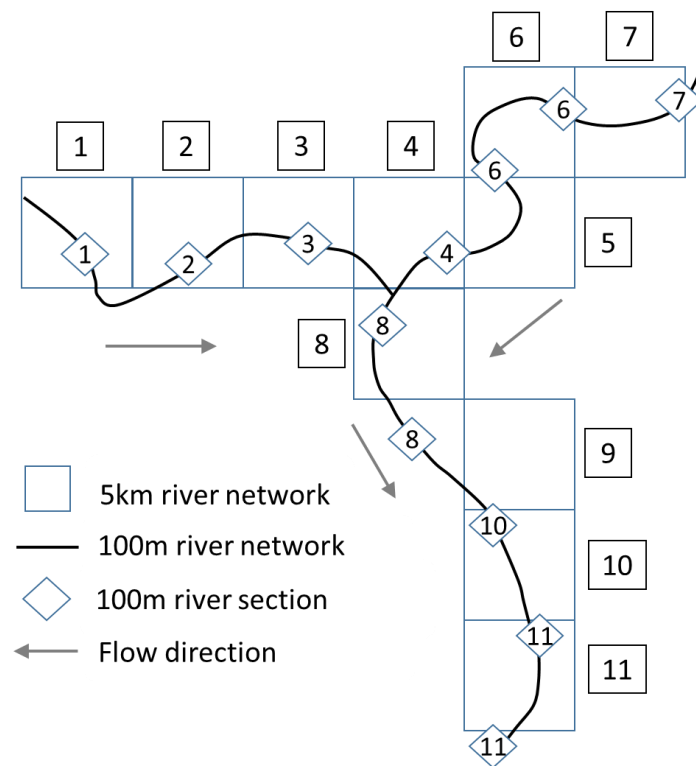
184 Because river channels are usually not represented in continental-scale topography, flood
 185 hydrograph values are reduced by subtracting the 2-year discharge peak $Q_{T(2)}$, which is commonly
 186 considered representative of river bank-full conditions. (Note that the original DEM is not
 187 modified with this procedure). Hence, the overall volume of the flood hydrograph is given by the
 188 sum of all daily flow values with duration $< T_c$.

189

190 **2.3 Flood hazard mapping**

191 The continental-scale flood hazard maps are derived from local flood simulations run along the
 192 entire river network, as in Alfieri et al. (2014). We use the DEM at 100 metres resolution
 193 developed for the Catchment Characterization and Modelling Database (CCM; Vogt et al., 2007)
 194 to derive a high-resolution river network at the same resolution. Along this river network we
 195 identify reference sections every 5 km along stream-wise direction, and we link each section to
 196 the closest upstream section (pixel) of the EFAS 5 km river network, using a partially automated
 197 procedure to ensure a correct linkage near confluences. In this way, the hydrological variables
 198 necessary to build the flood hydrographs can be transferred from the 5 km to the 100 metres river
 199 network. Figure 3 describes how the 5 km and 100 metres river sections are linked using a
 200 conceptual scheme.

201 Then, for every 100 metres river section we run flood simulations using the two-dimensional
 202 hydrodynamic model LISFLOOD-FP (Shaw et al., 2021), to produce a local flood map for each
 203 of the six reference return periods. Simulations are based on the local inertia solver of
 204 LISFLOOD-FP developed by Bates et al. (2010), which is now available as open-source software
 205 (<https://www.seamlesswave.com/LISFLOOD8.0>). We use the CCM DEM as elevation data, the
 206 synthetic hydrographs described in Section 2.2 as hydrological input data, and a mosaic of
 207 CORINE Land Cover for the year 2016 (Copernicus LMS, 2017) and Copernicus GlobCover
 208 (Global Land Cover Map) for the year 2009 (Bontemps et al., 2009) to estimate the friction
 209 coefficient based on land use.
 210 Finally, the flood maps with the same return period are merged together to obtain the continental-
 211 scale flood hazard maps. The 100 metres river network is included as a separate map in the dataset,
 212 to delineate those water courses that were considered in creating the flood hazard maps.



213
 214 *Figure 3. Conceptual scheme of the EFAS river network (5 km, squares) with the high-resolution*
 215 *network (100 metres) and river sections (diamonds) where flood simulations are derived. The*
 216 *related sections of the two networks are indicated by the same number. Source: Dottori et al.*
 217 *(2017).*

218

219 It is important to note that the flood maps developed do not account for the influence of local
220 flood defences, in particular dyke systems. Such limitation has been dictated mainly by the
221 absence of consistent data at European scale. None of the available DEMs for Europe has the
222 required accuracy and resolution to embed artificial embankments into elevation data.
223 Furthermore, there are no publicly available continental or national datasets describing the
224 location and characteristics (e.g. dyke height, distance from river channel) for flood protections.
225 Currently available datasets are based on the design return period of flood protection, e.g. the
226 maximum return period of flood events that protections can withstand before being overrun,
227 (Jongman et al., 2014; Scussolini et al., 2016). Most of the protection standards reported by these
228 datasets for Europe are based on empirical regressions derived using proxy variables (e.g. GDP,
229 land use), with few data based on actual design standards. While these datasets have been applied
230 to calculate flood risk scenarios (Alfieri et al., 2015) and flood impacts (Dottori et al., 2017), they
231 have important limitations when used for mapping flood extent. Wing et al. (2017) linked the
232 flood return period of protection standards with flood frequency analysis to adjust the bank height
233 of the river channels, however with impaired performance of the model. Moreover, recent studies
234 for United States suggest that empirical regressions based on gross domestic product and land use
235 may not be reliable (Wing et al., 2019).
236 Despite these limitations, maps not accounting for physical flood defences may be applied to
237 estimate the flood hazard in case of failure of the protection structures, and for flood events
238 exceeding protection levels.

239 *2.3 Validation of flood hazard maps*

240 *2.3.1 Selection of validation areas and maps*

241 The validation of large-scale flood hazard maps requires the use of benchmarks with one or more
242 datasets with extension and accuracy commensurate to the modelled maps. For instance Wing et
243 al. (2017) used the official hazard maps developed for the conterminous United States to evaluate
244 the performance of two flood hazard models, respectively designed to produce global- and
245 continental-scale flood maps (see Section 1). In Europe, all EU Member States as well as the UK
246 have developed national datasets of flood hazard maps for a range of flood probabilities (usually
247 expressed with the flood return period), following the guidelines of the EU Floods Directive (EC

248 2007). These maps are usually derived using multiple hydrodynamic models of varying
249 complexity (AdB Po, 2012) based on high-resolution topographic and hydrological datasets, such
250 as DEMs of at least 5 metres resolution in England (Sampson et al., 2015), LIDAR elevation data
251 in Spain (MITECO 2011), and river sections based on LIDAR surveys in the Po River basin (AdB
252 Po, 2012). Although official maps might be either prone to errors or incomplete (Wing et al 2017),
253 these are likely to provide a higher accuracy than the modelled maps presented here, and therefore
254 they have been selected as reference maps for the validation. While official flood maps are
255 generally available online for consultation on Web-GIS services, only few countries and river
256 basin authorities make the maps available for download in a format that allows comparison with
257 geospatial data. Table 1 presents the list of flood hazard maps that could be retrieved and used for
258 the validation exercise, while their geographical distribution is shown in Figure 1. Note that the
259 relevant links to access these maps are provided in the Data Availability section.

260 While more of such official maps are likely to become available in the near future, the maps
261 considered here offer an acceptable overview of the different climatic zones and floodplain
262 characteristics of the European continent. Conversely, we could not retrieve national or regional
263 flood hazard maps outside Europe, meaning the skill of the modelled maps could not be tested in
264 the arid regions in Northern Africa and Eastern Mediterranean. In Norway, Spain, the UK and the
265 Po River Basin the official maps take flood defences into account, which are not represented in
266 the modelling framework. Official maps for England also include areas prone to coastal flooding
267 events (such as tidal and storm surges). None of the official maps include areas prone to pluvial
268 flooding, which are therefore not considered in this analysis.

269 As mentioned in Section 2.3, the modelled maps do not include the effect of flood protections.
270 Wherever possible, for the comparison exercise we selected either reference flood maps that do
271 not account for protections (e.g. Hungary) or maps for flood return periods exceeding local
272 protection standards, assuming that the resulting flood extent is relatively unaffected by flood
273 defences. For example, the main stem of the Po river is protected against 1-in-200-year flood
274 events (Wing et al., 2019), whereas protection standards in England and Norway are usually
275 above 20 years (Scussolini et al., 2016). Reference maps where the extent and design level of
276 protection are not known (e.g. Spain) have been also included in the comparison to increase the
277 number of validation areas.

278

Country	Geographical extent	Return periods used	Defences included
Hungary	Country scale	30 - 100 – 1,000 years	No
Italy	Po River Basin	500 years	Yes
Norway	Country scale	100 years	Yes
Spain	Country scale	10 - 100 - 500 years	Yes
UK	England	100 – 1,000 years	Yes

279 *Table 1. Characteristics of the flood hazard maps used in the validation exercise. The links for*
280 *downloading the maps are provided in the Data Availability section.*

281 **2.3.2 Performance metrics and validation procedure**

282 The national flood hazard maps listed in Table 1 are provided as polygons of flood extent, with
283 no information on water depth or on original resolution of data. According to Sampson et al.
284 (2015), the official flood hazard maps for England are constructed using DEMs of at least 5 metres
285 resolution, therefore flood extent maps should be of comparable resolution. Reference flood maps
286 for the Po basin and Spain are likely to have a similar resolution since they are based on LIDAR
287 elevation data (AdB Po, 2012; MITECO 2011). For the comparison, official reference maps have
288 been converted to raster format with the same resolution as the modelled maps (i.e. 100 metres),
289 while the latter have been converted to binary flood extent maps. To improve the comparison
290 between modelled and reference maps we applied a number of corrections. Firstly, we used the
291 CORINE Land Cover map to exclude permanent water bodies (river beds of large rivers or
292 estuaries, lakes, reservoirs, coastal lagoons) from the comparison. Secondly, we restricted the
293 comparison area around modelled maps to exclude the elements of river network (e.g. minor
294 tributaries) included in the reference maps but not in the modelled maps. We used a different
295 buffer extent according to each study area, considering the floodplain morphology and the
296 variable extent and density of mapped river network. For example, in Hungary we applied a 10-
297 km buffer around modelled maps to include the large flooded areas reported in reference maps
298 and to avoid overfitting. In England, we used a 5 km buffer due to the high density of the river

299 network mapped in the official maps. The buffer is also applied to mask out coastal areas far from
 300 rivers estuaries, because official maps include flood-prone areas due to 1-in-200-year coastal
 301 flood events. We calculated that flood-prone areas inside the 5 km buffer correspond to 73% of
 302 the total extent for the 1-in-100-year flood. For the Po river basin, we excluded from the
 303 comparison the areas belonging to the Adige river basin and the lowland drainage network, which
 304 are not included in the official hazard maps. In Spain and Norway official flood hazard maps have
 305 only been produced where relevant assets are at risk, according to available documentation
 306 [MITECO 2011; NVE 2020]. We therefore restricted the comparison only to areas where official
 307 flood hazard maps have been produced. Table 2 provide the list of parameters used to determine
 308 the areas used for the comparison.

Test area	Buffer value (reference maps)	Buffer value (modelled maps)
Hungary	NA	10 km
Po River Basin	NA	See main text
Norway	5 km	5 km
Spain	5 km	5 km
England	NA	5 km

309 *Table 2. List of parameters used to determine the extent of areas used for comparing reference*
 310 *and modelled maps (NA: buffer not applied).*

311
 312 We evaluate the performance of simulated flood maps against reference maps using a number of
 313 indices proposed in literature (Bates and De Roo, 2000; Alfieri et al., 2014; Dottori et al., 2016b;
 314 Wing et al., 2017). The hit ratio (HR) evaluates the agreement of simulated maps with
 315 observations and it is defined as:

$$316 \quad HR = (Fm \cap Fo) / (Fo) \times 100 \quad (1)$$

317 where $Fm \cap Fo$ is the area correctly predicted as flooded by the model, and Fo indicates the total
 318 observed flooded area. HR scores range from 0 to 1, with a score of 1 indicating that all wet cells

319 in the benchmark data are wet in the model data. The formulation of the HR does not penalize
320 over-prediction, which can be instead quantified using the false alarm ratio FAR:

$$321 \quad FAR = (Fm/Fo)/(Fm) \times 100 \quad (2)$$

322 where Fm/Fo is the area wrongly predicted as flooded by the model. FAR scores range from 0
323 (no false alarms) to 1 (all false alarms). Finally, a more comprehensive measure of the agreement
324 between simulations and observations is given by the critical success index (CSI), defined as:

$$325 \quad CSI = (Fm \cap Fo)/(Fm \cup Fo) \times 100 \quad (3)$$

326 where $Fm \cup Fo$ is the union of observed and simulated flooded areas. CSI scores range from 0
327 (no match between model and benchmark) to 1 (perfect match between benchmark and model).

328 *2.4 Additional tests*

329 To choose the best possible methodologies and datasets to construct the flood hazard maps, we
330 performed a number of tests using recent input datasets, as well as alternative strategies to account
331 for vegetation effects on elevation data.

332 *2.4.1 Elevation data*

333 It is well recognized that the quality of flood hazard maps strongly depend on the accuracy of
334 elevation data used for modelling (Yamazaki et al., 2017). This is especially crucial for
335 continental-scale maps, since the quality of available elevation datasets is rarely commensurate
336 to the accuracy required for modelling flood processes [Wing et al., 2017]. Moreover, high-
337 resolution and accurate elevation data such as LIDAR-based DEMs cannot be used for reasons of
338 consistency, since these data are only available for few areas and countries.

339 The recent release of new global elevation models have the potential to improve the accuracy of
340 large-scale flood simulations, and hence the quality of flood hazard maps. Here, we test the use
341 of the MERIT DEM (Yamazaki et al., 2017) within the proposed modelling approach and we
342 compare the results with those obtained with CCM DEM. The MERIT DEM is based on the
343 SRTM data, similarly to CCM DEM, but has been extensively corrected and improved through
344 comparisons with other large-scale datasets, to eliminate error bias, improve data accuracy at high
345 latitudes (areas above 60° are not covered by SRTM), and compensate for factors like vegetation
346 cover. Note that areas above 60° in CCM DEM were derived from national datasets, and therefore
347 these areas are where the two datasets are likely to differ most.

348 *2.4.2 Correction of elevation data with land use*

349 The CCM DEM elevation dataset is mostly based on SRTM data, and so the elevation values can
350 be spuriously increased by the effect of vegetation canopy in densely vegetated areas, and by
351 buildings in urban areas. Recent research work has proposed advanced techniques to remove
352 surface artefacts, based on artificial neural networks (Wendi et al., 2016, Kulp and Strauss, 2018)
353 or other machine learning methods (Liu et al., 2018; Meadows and Wilson, 2021). Most
354 approaches correct DEM elevation with higher-accuracy datasets, using auxiliary data such as
355 tree density and height for correcting vegetation bias (as done for the MERIT-DEM by Yamazaki
356 et al., 2017), whereas elevation bias in urban areas can be corrected using night light, population
357 density, or OpenStreetMap elevation data (Liu et al., 2018). Given that improving elevation data
358 is not the main scope of this work, we opted for applying a simpler method for quickly correcting
359 the CCM DEM elevation data. Specifically, we use the land cover map derived from CORINE
360 Land Cover and Copernicus GlobCover to identify densely vegetated areas and urban areas, and
361 we applied a correction factor as a function of local land use to reduce elevation locally. The
362 correction factor varies from 8 metres for dense forested areas, to 2 metres for urban areas. Note
363 that these values are based on the findings of previous literature studies such as Baugh et al.
364 (2013) and Dottori et al. (2016b), while a formal calibration was not undertaken.

365

366 *3) Results and discussion*

367 We present the outcomes of the validation exercise by first describing the general results at
368 country and regional scale (Section 3.1). Then, we discuss the outcomes for England, Hungary
369 and Spain (Section 3.2), while the Norway and Po river basin case studies are presented in the
370 Appendix C. We also complement the analysis with additional validation over major river basins
371 in England and Spain. In Section 3.3 we compare our results with the validation exercise carried
372 out by Wing et al. (2017) and with the findings of other literature studies. Finally, in Section 3.4
373 and 3.5 (and Appendix B) we compare the performance of the present and previous versions of
374 the flood hazard map dataset, and we discuss the results of the tests with different elevation data
375 and strategies to account for vegetation.

376 *3.1 Validation of modelled maps at national and regional scale*

377 Table 3 presents the results of the validation for each testing area and return period. The
378 performance metrics are calculated using the total extent of the reference and modelled maps with
379 the same return period. The first visible outcome is the low scores for the comparisons with
380 reference maps with high probability of flooding, i.e. low flood return periods (< 30 years).
381 Performances improve markedly with the increasing of return periods due to the decrease of false
382 alarm rate (FAR), while the hit rate (HR) does not vary significantly. In particular, critical success
383 index (CSI) values approach 0.5 for the low probability flood maps, i.e., for return periods equal
384 or above 500 years. Considering that most of the reference flood maps include the effect of flood
385 defences (unlike the modelled maps), these results suggest that the majority of rivers in the study
386 areas may be protected for flood return periods of around 100 years or less, as indeed reported by
387 available flood defence databases (Scussolini et al., 2016). Differences between simulated and
388 reference hydrological input are likely to influence the skill of modelled flood maps and may
389 depend on several factors such as the hydrological model performance for peak flows, extreme
390 value analysis (distribution used for extreme value fitting, length of available time-series) design
391 hydrograph estimation. However, further analysis is difficult as we have no specific information
392 on the hydrological input used for the reference flood maps (e.g. peak flows, statistical modelling
393 of extremes, hydrograph shape). In the following Sections, we use the skill of the LISFLOOD
394 long-term simulation to evaluate the agreement between modelled and observed hydrological
395 regime, but this does not necessarily translate to extreme values. High-probability floods are also
396 sensitive to the method used to reproduce river channels, and the simplified approach used in this
397 study might underestimate the conveyance capacity of channels (see Section 3.2.2 for an
398 example). Finally, the better performance for low-probability floods may also depend on
399 floodplain morphology, where valley sides create a morphological limit to flood extent.

400

401

402

403

404

405 *Table 3. Results of the validation against official flood hazard maps: value of the performance*
 406 *indices at country and regional scale. RP=Return Period, HR=Hit Ratio, FAR= False Alarm*
 407 *Ratio, CSI=Critical Success Index.*

REGION	RP (years)	HR	FAR	CSI
Spain	10	0.58	0.65	0.28
Hungary	30	0.77	0.88	0.11
Spain	100	0.63	0.44	0.42
Hungary	100	0.76	0.74	0.24
Norway	100	0.70	0.72	0.25
England	100	0.53	0.31	0.43
Po River Basin	500	0.60	0.13	0.56
Spain	500	0.61	0.36	0.45
Hungary	1000	0.76	0.45	0.47
England	1000	0.52	0.12	0.48

408 *3.2 Discussion of results at national and regional scale*

409 The results in Table 3 highlight considerable differences in the skill of the flood maps across
 410 countries and regions. While some differences may arise from the variability of floodplain
 411 morphology and model input data, others are attributable to the different methods applied to
 412 produce the reference maps (MITECO 2011; NVE 2020). In the following sections we examine
 413 in more detail the outcomes for each study area.

414 *3.2.1 England*

415 According to Table 3, modelled flood maps tend to underestimate flood extent in England, as
 416 visible by the HR values around 0.5 (e.g. out of every two flooded cells, only one is correctly
 417 identified as flooded by the model). Such result is confirmed when focusing the analysis on the
 418 major river basins of England, as reported in Table 4. Notably, HR has generally marginal or no
 419 increases with the increase of return period considered, while FAR values have a marked
 420 decrease. The results of reported by Arnal et al. (2019) and summarized in Figure B1 suggest a
 421 fair hydrological skill of the LISFLOOD calibration in England, with KGE values generally above

422 0.5. However, there is not a clear correlation between hydrological and flood map skill, with some
 423 basins (e.g. Thames) showing high KGE values but relatively low CSI values.

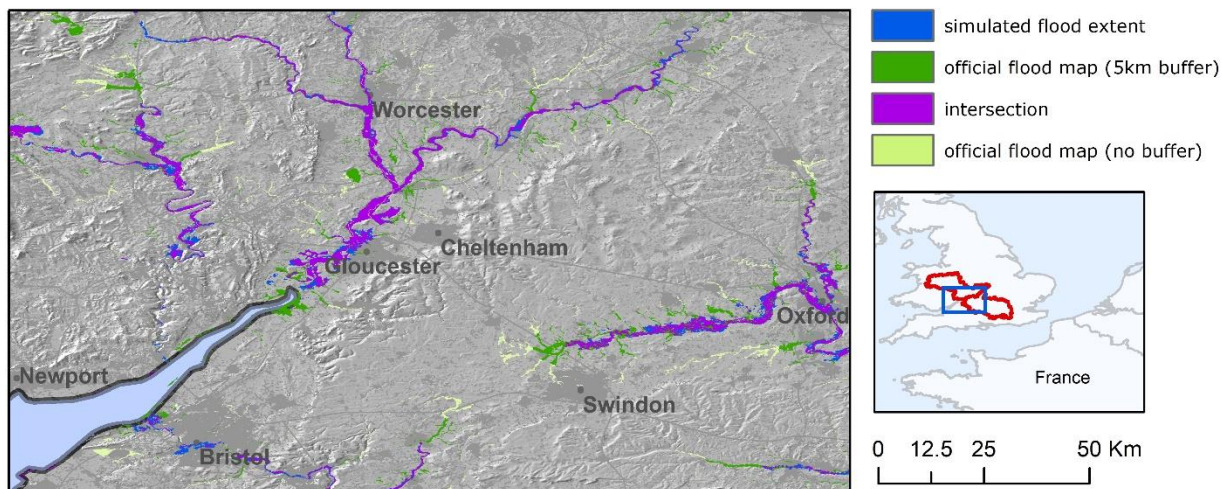
424 For the Thames basin, the low CSI value is likely influenced by the tidal flooding component
 425 from London eastwards. According to Sampson et al. (2015), the official flood hazard map
 426 assumes a 1 in 200 year coastal flood along with failure of the Thames tidal barrier, whereas our
 427 river flood simulations use the mean sea level as boundary condition and do include storm surge
 428 and tidal flooding. Concurrent fluvial-tidal flooding processes occur in other river estuaries, so
 429 this might reduce the skill of the modelled maps. Furthermore, the Thames catchment is heavily
 430 urbanized and has extensive flood defence and alleviation schemes compared the other
 431 catchments (Sampson et al., 2015). Both aspects might increase the elevation bias of CCM DEM
 432 and complicate the correct simulation of extreme flood events.

433 *Table 4. Validation indices in England and in major river basins.*

Catchments	100-year RP			1,000-year RP		
	HR	FAR	CSI	HR	FAR	CSI
England	0.53	0.31	0.43	0.52	0.12	0.48
Ouse	0.57	0.39	0.42	0.56	0.19	0.49
Severn	0.64	0.24	0.53	0.63	0.20	0.54
Thames, above Lea	0.56	0.46	0.38	0.55	0.23	0.47
Trent	0.63	0.28	0.50	0.59	0.06	0.57
Tyne	0.51	0.43	0.37	0.52	0.28	0.43

434
 435 Besides these results, the visual inspection of reference maps suggest that the underestimation is
 436 partly caused by the high density of mapped river network in the reference maps, in respect to
 437 modelled maps. Indeed, the modelling framework excludes river basins with an upstream basin
 438 area below 500 km², meaning that EFAS maps only cover main river stems but miss out several
 439 smaller tributaries. This is clearly visible over the Severn and in the upper Thames basins (Figure
 440 4), and might also explain the lower skill in the lowlands of Ouse and Trent rivers, where the
 441 contributions of main river stems and tributaries to the flood extent are difficult to separate.
 442 Including minor tributaries in the flood maps would require either to increase the resolution of
 443 the climatological forcing to reproduce intense local rainfall, or to add a pluvial flooding
 444 component as done by Wing et al. (2017). Finally, areas prone to storm surge and tidal flooding

445 around river estuaries might further reduce the overall skill of modelled maps, despite the 5 km
446 buffer applied.



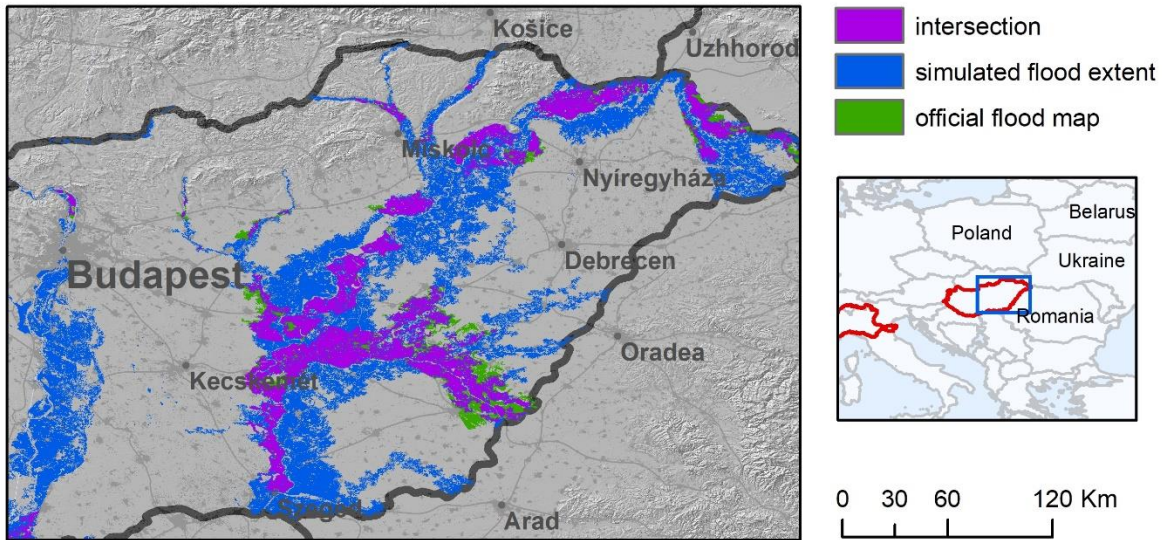
447
448 *Figure 4. Comparison of modelled (blue) and reference (green) flood hazard maps (1-in-100-*
449 *year) over the Severn (centre) and the upper Thames (right) river basins in England. Purple*
450 *areas denotes intersection (agreement) between the modelled and reference set of maps. The*
451 *original reference maps (i.e. with no masking around modelled maps) are shown in light green.*
452

453 3.2.2 Hungary

454 The results in Table 3 for Hungary show a general tendency to overestimate flood extent for all
455 return periods. HR values are consistently high and do not change much with the return period.
456 Conversely, FAR is very high for the 1-in-30 year flood map and still considerable even for the
457 1-in-1000 year flood map. Arnal et al (2019) reported a fair hydrological skill of LISFLOOD
458 (KGE values >0.5) for the calibration period, even though KGE validation values were
459 considerably low for the Tisza River.

460 Given that flood defences are not modelled in reference maps, the observed results may be
461 explained by assuming a large conveyance capacity of river channels. For instance, the 1-in-100
462 year reference map show relatively few flooded areas for the Danube main stem (Figure 5), thus
463 suggesting that the main channels can convey the 1-in-100-year discharge without overflowing.
464 Conversely, river channels in the modelling framework are assumed to convey only the 1-in-2-
465 year discharge. Obviously, the same considerations can be made for 1-in-30-year discharge for

466 the majority of river network, which explains the very low scores. Furthermore, artificial
 467 structures such as road embankments and drainage network may further reduce flood extent in
 468 lowland areas, leading to further overestimation given the fact that these features are not
 469 represented in the DEM. These findings highlight the need for high-resolution DEM fed with
 470 local-scale information to achieve adequate performance in lowland areas, as observed also by
 471 Wing et al (2019b).



472
 473 *Figure 5. Comparison of modelled (blue) and reference (green) flood hazard maps (1-in-100-*
 474 *year) over the Danube (left) and Tisza (right) rivers in Hungary. Purple areas denotes the*
 475 *intersection between the modelled and reference set of maps.*

476

477 3.2.3 Spain

478 The performance of the modelled maps in Spain show a fairly stable HR value and decreasing
 479 FAR values with increasing return periods, similarly to what was observed for England and
 480 Hungary. The analysis of the results for the major river basins of the Iberian Peninsula, reported
 481 in Table 5, provide further insight on the skill of flood maps. A number of basins exhibit both
 482 large HR and FAR such as the Duero, Tajo and Guadalquivir basins. Rivers in South-East Spain
 483 (Segura, Jucar) have relatively low HR values, while the modelled maps perform better in the
 484 Ebro river basin. The interpretation of results requires the consideration of different aspects. The
 485 poor results for the 1-in-10-year maps are likely due to the effect of flood protection structures,
 486 such as dykes and flood regulation systems, which are probably relevant also for the 1-in-100-

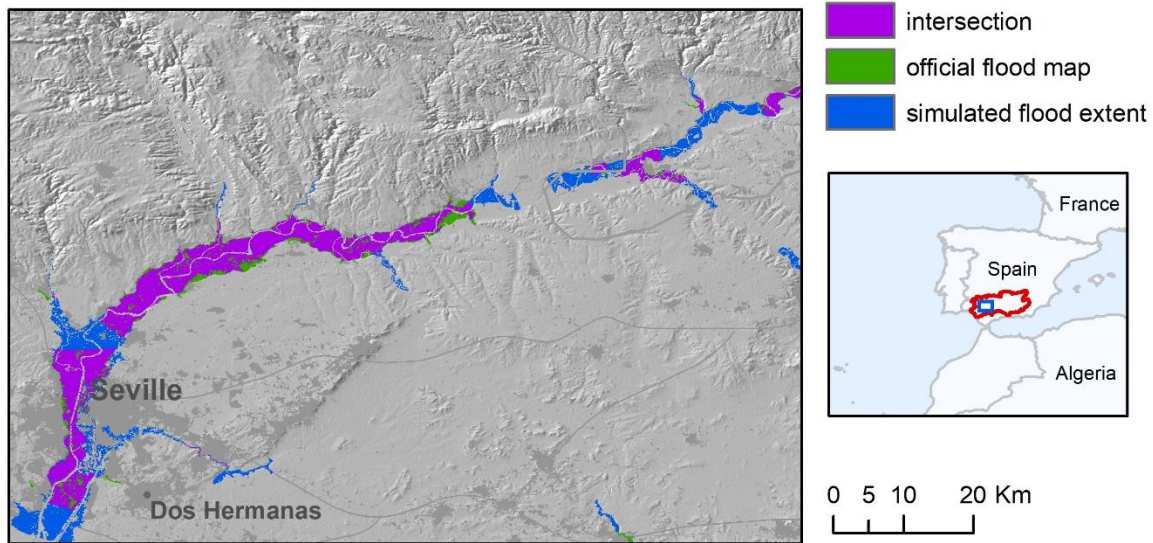
487 year map. Indeed, most Iberian rivers are regulated by multiple reservoirs, which are often used
 488 to reduce flood peaks according to specific operating rules. While dykes are not represented in
 489 the inundation model, reservoirs are included in the LISFLOOD model through a simplified
 490 approach, given that operating rules are not known. Therefore, the real and modelled hydrological
 491 regimes might differ significantly, including flow peaks of low-probability flood events. This is
 492 reflected also by the low hydrological skill of LISFLOOD, with KGE values generally below 0.5
 493 with few exceptions (Figure B1).

494 In addition, the comparison of modelled and reference maps is affected by the partial coverage of
 495 the reference inundation maps in several river basins. According to the information available in
 496 the official website (MITECO 2011) large sections of the river network in the basins of the Duero,
 497 Tajo, Guadiana and Guadalquivir rivers have not been analysed, due to the absence of relevant
 498 assets or inhabited places at risk. Even though this has been accounted by restricting the area of
 499 comparison around reference maps, a visual inspection of the maps being compared shows
 500 spurious overestimation around the edges of reference map polygons (Figure 6). Finally, the low
 501 HR values scored in rivers in South-East Spain (Segura, Jucar) are partially explained by the
 502 presence of several tributaries not included in EFAS maps.

503

504 *Table 5. Validation indices in Spain and in some test river basins.*

Catchments	10-year RP			100-year RP			500-year RP		
	HR	FAR	CSI	HR	FAR	CSI	HR	FAR	CSI
Spain	0.58	0.65	0.28	0.63	0.44	0.42	0.61	0.36	0.45
Duero	0.60	0.74	0.22	0.65	0.55	0.36	0.65	0.46	0.42
Ebro	0.71	0.46	0.45	0.75	0.27	0.59	0.74	0.23	0.61
Guadalquivir	0.67	0.66	0.29	0.69	0.49	0.42	0.66	0.46	0.42
Guadiana	0.52	0.63	0.28	0.60	0.42	0.42	0.61	0.31	0.48
Jucar	0.32	0.89	0.09	0.53	0.46	0.36	0.51	0.39	0.39
Tajo	0.60	0.85	0.14	0.70	0.63	0.32	0.69	0.49	0.41
Segura	0.18	0.89	0.07	0.38	0.52	0.27	0.41	0.24	0.36



505
 506 *Figure 6. Comparison of modelled (blue) and reference (green) flood hazard maps (1-in-100-*
 507 *year) over a stretch of the Guadalquivir river basin, Spain. Purple areas denote the intersection*
 508 *between the two set of maps.*

509 **3.3 Comparison with previous continental-scale validation studies**

510 To put the previously described results in context, we compare them with the validation exercises
 511 performed by Sampson et al. (2015) over the Thames and Severn rivers in England, and by Wing
 512 et al. (2017) over United States. The study by Wing et al. is, to our knowledge, the first study that
 513 carried out a consistent validation of modelled flood hazard maps at continental scale. Bates et al.
 514 (2021) have recently updated the work by Wing et al. by including pluvial and coastal flooding
 515 components in the modelling framework, but their work is not considered here. A comparison of
 516 validation metrics of the three studies are shown in Table 6 and 7. For our framework, we
 517 calculated each index in Table 6 using the overall modelled and reference flood extent available
 518 for each return period (e.g. the value for the 100-year maps includes reference and modelled maps
 519 for England, Spain and Norway). As such, each area is weighted according to the extent of the
 520 corresponding flood map.

521 As can be seen in Table 6, the continental-scale model by Wing et al. achieved the highest scores
 522 both for 100-year and 500-year return periods. However, this model is based on national datasets
 523 with higher accuracy and resolution than those available for the European continent (e.g. a 10
 524 metres resolution DEM and a detailed catalogue of flood defences). The global and European

525 models have comparable hit rates for the 100-year flood maps (0.68 and 0.65 respectively), but
 526 the former exhibits a much lower FAR value (0.34 compared to 0.61 for the European model),
 527 and a higher HR value for the 500-year maps.

528 The higher HR values scored by the US and global models might depend on the higher density of
 529 the modelled river network, which includes river reaches up to 50 km² by simulating both pluvial
 530 and fluvial flooding processes. The lower FAR values of the US and global models might be
 531 explained by the inclusion of flood defences. In the US model, defences are explicitly modelled
 532 using the US dataset of flood defences, while the global model parameterizes flood defences
 533 through the adjustment of channel conveyance using socioeconomic factors and degree of
 534 urbanization (Wing et al., 2017). However, Wing et al observed that the latter methodology had
 535 a negligible effect on HR values in defended areas, when compared with an undefended version
 536 of the model.

537 Another possible reason for the low FAR values is the different approach used in the validation
 538 method. Wing et al. applied a narrow 1 km buffer around official maps to constrain the area of
 539 comparison and avoid spurious over-prediction in areas not considered by official maps.
 540 However, this might result in a reduction of true false alarms, because part of overestimated flood
 541 areas can go undetected. To verify this hypothesis, we recalculated the performance indices
 542 against the 100-year reference map in Spain using a 1 km buffer instead of the 5 km previously
 543 applied to constrain the validation area. As a result the FAR dropped from 0.44 to 0.34, similar
 544 to the performance of the global model. However, we observed a reduction of true false alarms,
 545 especially in river basins with continuous map coverage such as the Ebro, Jucar and Segura.

546 *Table 6. Comparison of the performance metrics for the European model described in the present*
 547 *study and the two models evaluated in the study by Wing et al. (2017).*

	RP (years)	HR	FAR	CSI
US model (Wing et al.)	100	0.82	0.37	0.55
Global model (Wing et al.)	100	0.69	0.34	0.50
European model (this study)	100	0.66	0.61	0.32
US model (Wing et al.)	500	0.86	na	na
Global model (Wing et al.)	500	0.74	na	na
European model (this study)	500	0.61	0.24	0.51
European model (this study)	1000	0.68	0.39	0.47

548

549 The comparison of HR, FAR and CSI values show better scores for the global maps by Sampson
550 et al. (2015) in respect to our modelled maps (Table 7).

551

552 *Table 7. Comparison of the performance metrics for the maps described in the present study and*
553 *the global maps by Sampson et al. (2015). Metrics for the latter study are calculated removing*
554 *all channels with upstream areas of less than 500 km².*

	HR	FAR	CSI
Thames (this study)	0.56	0.46	0.38
Thames (Sampson et al. 2015)	0.73	0.3	0.56
Severn (this study)	0.64	0.24	0.53
Severn (Sampson et al. 2015)	0.83	0.23	0.67

555

556 The different masking applied to reference flood maps may explain some of the differences:
557 Sampson et al. removed all channels with upstream areas of less than 500 km², whereas here we
558 use a simpler 5 km buffer around modelled maps. The exclusion of permanent river channels in
559 our comparison may further penalize the overall score especially for the Thames, which as a rather
560 large channel estuary. Besides these differences in the validation, the better metrics of the maps
561 by Sampson et al. may depend on a more accurate hydrological input (based on regionalization
562 of gauge station data) and a better correction of urban elevation bias (based on a moving window
563 filter instead of the constant correction values applied here).

564 To provide further context, the US model by Wing et al. (2017) attained average CSI values of
565 ~0.75 against a number of detailed local models, whereas flood models built and calibrated for
566 local applications may achieve CSI scores up to 0.9 when benchmarked against very high quality
567 data (see Wing et al., 2019a). Fleischmann et al. (2019) recently proposed that regional-scale
568 models can provide locally relevant estimates of flood extent when CSI > 0.65. Although the
569 overall values shown in Table 3 are consistently below this threshold, better results are observed
570 for a number of river basins, as shown in Tables 4 and 5.

571

572

573 **3.4 Comparison with the previous flood map dataset**

574 Table 7 compares the performances of the flood hazard maps described in the present study
 575 (version 2) with the previous version developed by Dottori et al. (2016a; version 1). The
 576 comparison is shown for England and Hungary. Results for all other areas are comprised within
 577 the range of results shown in Table 3. As can be seen, differences are generally reduced across
 578 the different areas and return periods. Version 1 of the flood maps produced slightly better results
 579 in Hungary for the 100- and 1000-year return period (increased CSI and HR, lower FAR), while
 580 version 2 has somewhat improved performances in England, mainly driven by higher HR.

581

582 *Table 7. Comparison of performances of the flood hazard maps described in the present study*
 583 *and developed by Dottori et al. (2016a). Table reports the ratio between flood extents (F2/F1)*
 584 *and the difference between Version 2 and 1 of the HR, FAR and CSI values.*

	RP (years)	F2/F1	ΔHR	ΔFAR	ΔCSI
Hungary	30	0.97	-0.5%	-0.4%	2.9%
Hungary	100	1.00	-2.1%	0.7%	-2.4%
Hungary	1000	1.01	-3.6%	5.7%	-6.3%
England	100	1.05	9.4%	1.7%	7.3%
England	1000	1.04	8.2%	-1.1%	7.7%

585

586 These outcomes may be interpreted considering the changes in input data between the two
 587 versions, and the structure of the modelling approach and of input data, which in turn has not
 588 changed substantially. The main difference between the two map versions is given by the
 589 hydrological input, with Version 2 using the latest calibrated version of the LISFLOOD model.
 590 For the 100-year return period, peak flow values of Version 2 are on average 35% lower than
 591 Version 1 in Hungary, and 16% lower in England. However, similar decreases are also observed
 592 for the 1-in-2-year peak discharge that determines full-bank discharge. The resulting reduction in
 593 channel hydraulic conveyance in respect to Version 1 is likely to offset the decrease of peak flood
 594 volumes, which explain the small difference in overall flood extent given by the F2/F1 parameter
 595 in Table 7. Such results confirm the low sensitivity of the modelling framework to the
 596 hydrological input observed by Dottori et al. (2016) and by Trigg et al (2016) for a global-scale
 597 application. It also confirms that the knowledge of river channel geometry is crucial to correctly

598 model the actual channel conveyance and thus improve inundation modelling. Other differences
 599 in input data are given by minor changes in Manning’s parameters and in the EFAS river network,
 600 which might contribute to the observed differences.

601

602 *3.5 Influence of elevation data*

603 Table 8 compares the metrics calculated with CCM DEM elevation data against the same metrics
 604 for the modelled flood maps based on MERIT-DEM. The comparison is carried out for England,
 605 Hungary and the Po river basin. Performance is slightly improved by the use of MERIT-DEM
 606 data for all areas and return periods, in particular through the reduction of FAR, even though the
 607 overall increase of CSI values is limited to few percentage points.

608

609 *Table 8. Comparison of performances of the flood hazard maps described in the present study*
 610 *and developed by Dottori et al. (2016a) based on the MERIT-DEM (a) and CCM-DEM (b). Table*
 611 *reports the ratio between flood extents F and the differences for HR, FAR, and CSI (e.g. (HRa-*
 612 *HRb)/HRa).*

	RP (years)	ΔF	ΔHR	ΔFAR	ΔCSI
Hungary	100	-5.3%	0.0%	-2.0%	5.1%
Hungary	1000	-5.9%	-0.1%	-7.6%	5.2%
England	100	0.0%	2.6%	-5.7%	3.8%
England	1000	1.7%	2.8%	-7.8%	3.2%
Po	500	0.2%	0.9%	-4.3%	3.4%

613

614 Because of this limited improvement and the considerable amount of time required to re-run the
 615 complete set of flood hazard maps (several days for each return period) it was decided not to
 616 update the flood maps using the MERIT-DEM as elevation data. Moreover, new high-resolution
 617 datasets such as the Copernicus DEM (ESA-Airbus 2019), the 90m version of TanDEM-X dataset
 618 (<https://geoservice.dlr.de/web/dataguide/tdm90>), and MERIT-HYDRO (Yamazaki et al., 2019)
 619 have recently become available, and therefore future research could focus on performing
 620 additional comparisons to identify which dataset is most suitable for inundation modelling in
 621 Europe.

623 *4) Conclusions and ongoing work*

624 We presented here a new dataset of flood hazard maps covering the geographical Europe and
625 including large parts of the Middle East and river basins entering the Mediterranean Sea. This
626 dataset significantly expands the previous available flood maps datasets at continental scale
627 (Alfieri et al., 2014; Dottori et al., 2016a), and therefore constitutes a valuable source of
628 information for future research studies and flood management, especially for countries where no
629 official flood hazard maps are available. The new maps also benefit of updated models and new
630 calibration and meteorological data. The maps are being used for a range of applications at
631 continental scale, from evaluating present and future river flood risk scenarios, to the cost-benefit
632 assessment of different adaptation strategies to reduce flood impacts, and for comparisons
633 between different regions, countries and river basins (Dottori et al, 2020b). Moreover, the flood
634 hazard maps are designed to be integrated with the Copernicus European Flood Awareness
635 System (EFAS), and will be used to perform operational flood impact forecasting in EFAS
636 (Dottori et al., 2017).

637 We performed a detailed validation of the modelled flood maps in several European countries
638 against official flood hazard maps. The resulting validation exercise is the most complete
639 undertaken so far for Europe to our best knowledge, and provided a comprehensive overview of
640 the strengths and limitations of the new maps. Nevertheless, the unavailability of reference flood
641 maps outside Europe did not allow any validation in the arid regions in North Africa and Eastern
642 Mediterranean. In these areas, further research will be needed to better understand the
643 performance of the flood mapping procedure here proposed. Modelled maps generally achieve
644 low scores for high and medium probability of flooding. For the 1-in-100-year return period, the
645 modelled maps can identify on average two-thirds of reference flood extent, however they also
646 largely overestimate flood-prone areas in many regions, thus hampering the overall performance.
647 Performances improves markedly with the increasing of return period, mostly due to the decrease
648 of the false alarm rates. In particular, critical success index (CSI) values approach and in some
649 cases exceed 0.5 for return periods equal or above 500 years, meaning that the maps can correctly
650 identify more than half of flooded areas in the main river stems and tributaries of different river
651 basins.

652 It is important to note that the validation was affected by problems in identifying the correct areas
653 for a fair comparison, because of the different density of the mapped river network in reference
654 and modelled maps. In our study we used large buffers to constrain comparison areas, which
655 possibly penalized the model performance by generating spurious false alarms in areas not
656 considered by official maps. However, we observed that the proposed maps achieve comparable
657 results to other large-scale flood models when using similar parameters for the validation.
658 The low skill of modelled maps for high and medium probability of flooding, with large
659 overestimations observed in different lowland areas, is likely motivated by the non-inclusion of
660 flood defences in the modelling framework and the simplified representation of channel hydraulic
661 conveyance, due to the absence of datasets at European scale describing river channels and
662 defence structures (i.e. design standards and location of dyke systems). Such information
663 combined with high-resolution DEM fed with local-scale information (artificial and defence
664 structures) is crucial to improve the performance of large-scale flood models and apply more
665 realistic flood modelling tools, as observed also by Wing et al (2017, 2019b). Uncertainty in peak
666 flow estimation can also influence the skill of the modelled maps; however, we found that the
667 limited sensitivity of the modelling approach to changes in the hydrological input smooths out
668 this uncertainty source, because channel conveyance is linked to streamflow characteristics. Such
669 finding highlight the need for independent data of river channel width, shape and depth to better
670 reproduce streamflow and flooding processes. Moreover, the improved results offered by the use
671 of the MERIT-DEM elevation data suggest that recent high-resolution datasets such as the
672 Copernicus DEM (ESA-Airbus 2019), TanDEM-X
673 (<https://geoservice.dlr.de/web/dataguide/tdm90>), and MERIT-HYDRO (Yamazaki et al., 2019)
674 may offer a viable solution to improve future versions of continental-scale flood hazard maps in
675 Europe.
676 Increasing map coverage by including the minor river network is likely to improve the skill of
677 modelled maps. However, this might require the use of a different modelling approach to account
678 for pluvial flooding (Wing et al., 2017; Bates et al., 2021), along with reliable model climatology
679 to represent small-scale precipitation processes. Improving the simulation of reservoirs may also
680 reduce the difference between the real and modelled hydrological regimes in regions such as the
681 Iberian Peninsula and the Alps.

682 *Data availability*

683 The dataset described in this manuscript is accessible as part of the data collection “Flood Hazard
684 Maps at European and Global Scale” at the JRC Data Catalogue
685 (<https://data.jrc.ec.europa.eu/collection/floods/>).

686 Please refer to the dataset as follows: Dottori F., Bianchi A., Alfieri, L., Skoien, J., Salamon P.,
687 2020. River flood hazard maps for Europe and the Mediterranean Basin. JRC Data Catalogue,
688 accessible at <http://data.europa.eu/89h/1d128b6c-a4ee-4858-9e34-6210707f3c81> , doi:
689 10.2905/1D128B6C-A4EE-4858-9E34-6210707F3C81

690 Note that the DOI for the dataset will be available soon. The dataset comprises the following
691 maps (eight in total), each one available as a raster (Geotiff) file:

- 692 • Map of permanent water bodies for Europe and the Mediterranean Basin
- 693 • River network in Europe and the Mediterranean Basin
- 694 • River flood hazard maps for Europe and the Mediterranean Basin (return periods of 10, 20,
695 50, 100, 200 and 500 years)

696 The official flood hazard maps used for the validation exercise are freely accessible at the
697 following web-sites:

- 698 • Spain: <https://www.miteco.gob.es/es/cartografia-y-sig/ide/descargas/agua/zi-lamina.aspx> (in
699 Spanish)
- 700 • Po River Basin: <https://pianoalluvioni.adbpo.it/progetto-esecutivo-delle-attivita/> (in Italian)
- 701 • Norway: <https://www.nve.no/flaum-og-skred/kartlegging/flaum/> (in Norwegian)
- 702 • England: [https://data.gov.uk/dataset/bed63fc1-dd26-4685-b143-2941088923b3/flood-map-](https://data.gov.uk/dataset/bed63fc1-dd26-4685-b143-2941088923b3/flood-map-for-planning-rivers-and-sea-flood-zone-3)
703 [for-planning-rivers-and-sea-flood-zone-3](https://data.gov.uk/dataset/bed63fc1-dd26-4685-b143-2941088923b3/flood-map-for-planning-rivers-and-sea-flood-zone-3) ; [https://data.gov.uk/dataset/cf494c44-05cd-4060-](https://data.gov.uk/dataset/cf494c44-05cd-4060-a029-35937970c9c6/flood-map-for-planning-rivers-and-sea-flood-zone-2)
704 [a029-35937970c9c6/flood-map-for-planning-rivers-and-sea-flood-zone-2](https://data.gov.uk/dataset/cf494c44-05cd-4060-a029-35937970c9c6/flood-map-for-planning-rivers-and-sea-flood-zone-2) (in English)
- 705 • Hungary: <https://www.vizugy.hu/index.php?module=content&programelemid=62> (in
706 Hungarian)

707 The LISFLOOD hydrological model used in this research is released as open-source software and
708 available at <https://ec-jrc.github.io/lisflood/>.

709 The streamflow dataset derived from the long-term run of the LISFLOOD model is available at
710 <https://cds.climate.copernicus.eu/cdsapp#!/dataset/efas-historical>

711 The LISFLOOD-FP hydrodynamic model used in this research is available as open-source
712 software at <https://www.seamlesswave.com/LISFLOOD8.0> for research and non-commercial
713 purposes.

714

715 *Appendix A: Meteorological observations used for LISFLOOD simulations*

716 The long-term run of the hydrological model LISFLOOD is based on observed data from
717 meteorological stations and precipitation datasets, which are collected and continuously expanded
718 as part of the development work for EFAS. The meteorological variables considered are:
719 precipitation, minimum and maximum temperature, wind speed, solar radiation and vapour
720 pressure. The number of stations with available meteorological observations depends on the
721 period and variable considered, with an increasing availability towards the end of the historical
722 simulation period. As an example, for the year 2016 the number of daily observations available
723 ranged from ~8.800 for temperature to ~5.500 for precipitation and ~3.700 for vapour pressure.
724 The input from meteorological stations is completed by a number of precipitation datasets
725 (EURO4M-APG, INCA-Analysis Austria, ERA-Interim GPCP corrected and Carpat-Clim; for
726 details see Arnal et al., 2019). Note that the same datasets are used to drive the LISFLOOD
727 calibration and to calculate the initial conditions for the EFAS forecasts. The data from
728 meteorological stations and gridded datasets were then interpolated using the interpolation
729 scheme SPHEREMAP to produce meteorological grids with a daily time step. The reader is
730 referred to Arnal et al. (2019) for further details.

731

732 *Appendix B: LISFLOOD calibration and validation results*

733 We report here an overview of the results of the LISFLOOD calibration and validation presented
734 by Arnal et al. (2019). The skill of LISFLOOD in reproducing observed flow regimes
735 (hydrological skill) is expressed using two indices, the Kling-Gupta Efficiency (KGE; Gupta et
736 al., 2009) and the Nash-Sutcliffe Efficiency (NSE; Nash and Sutcliffe, 1970). The NSE index is
737 widely applied in literature and is useful to measure the hydrological skill under high-flow
738 conditions, given its sensitivity to flow extremes (Krause et al., 2005). The KGE index provides

739 a more complete evaluation of the model skill under variable flow conditions, and is therefore
 740 useful for calibration purposes (Gupta et al., 2009; Knoben et al., 2019)

741 Table B1 summarizes the results of KGE and NSE indices, and Figure B1 shows the spatial
 742 distribution of the KGE index values across the EFAS domain. The spatial distribution of NSE is
 743 roughly similar. For a detailed list of scores for all stations, please refer to Arnal et al. (2019).

744

745 *Table B1. Overview of the hydrological skill of LISFLOOD for the calibration and validation*
 746 *stations.*

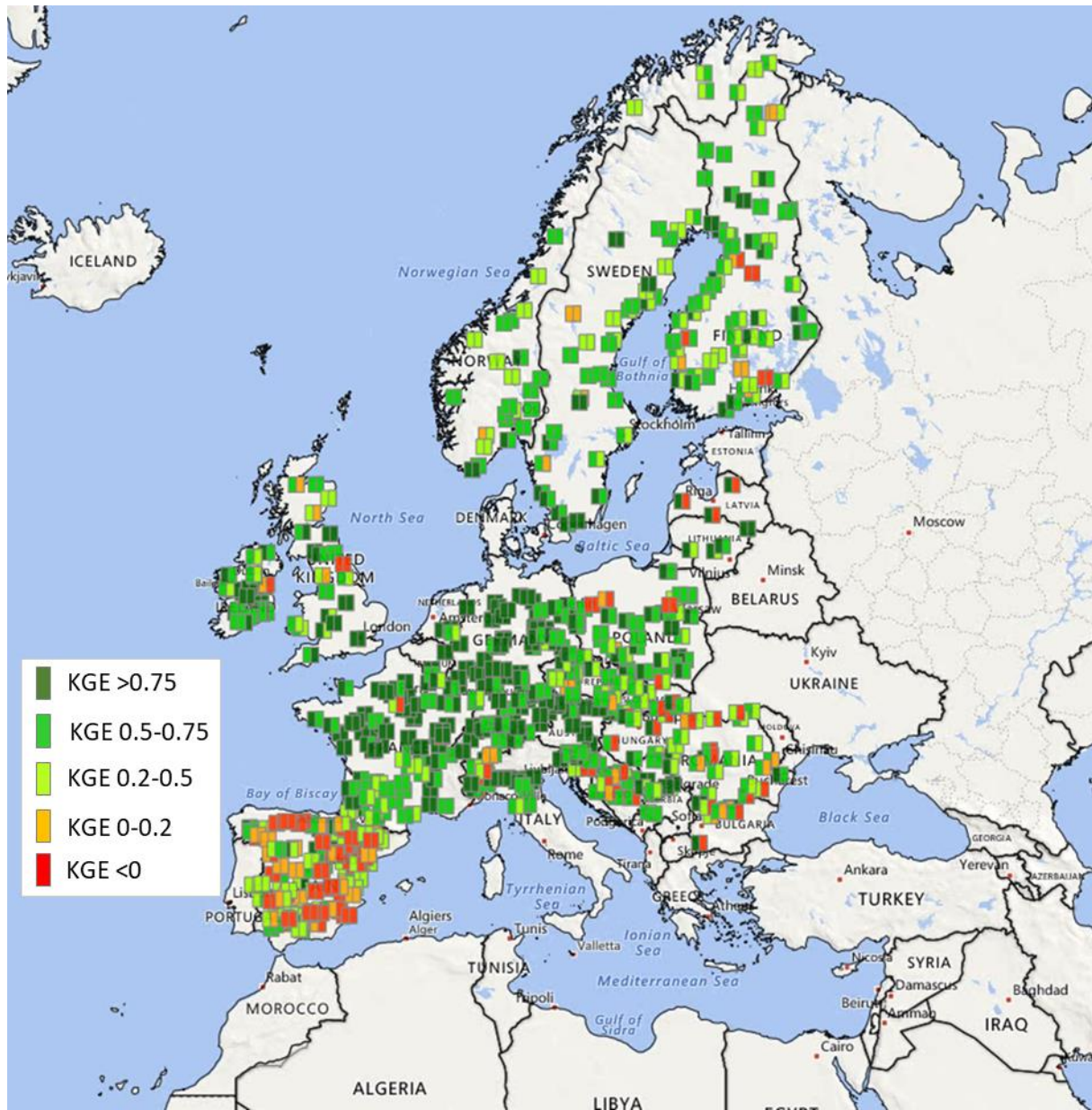
NSE	calibration		validation		KGE	calibration		validation	
	no. of stations	[%]	no. of stations	[%]		no. of stations	[%]	no. of stations	[%]
> 0.75	147	21%	101	14%	> 0.75	303	42%	174	24%
> 0.5–0.75	277	39%	207	30%	> 0.5–0.75	240	33%	235	33%
> 0.2–0.5	165	23%	171	25%	> 0.2–0.5	91	13%	172	24%
> 0–0.2	35	5%	65	9%	> 0–0.2	36	5%	44	6%
≤0	93	13%	153	22%	≤0	47	7%	73	10%
	∑ 717		∑ 698			∑ 717		∑ 698	

747

748 As can be seen from Table B1, 75 % of all stations scored a KGE higher than 0.5 during
 749 calibration, and 57 % during validation. NSE index values above 0.5 are scored for 60% and 44%
 750 of stations, respectively for the calibration and validation periods.

751 It is clearly noticeable that the skill is not homogeneously distributed across Europe, with higher
 752 skills in large parts of Central Europe, and lower skill mostly in Spain caused by the strong
 753 influence of reservoirs and flow control structures. The other study areas considered in the
 754 validation exercise (England, Hungary, Norway, Po river basin) exhibit KGE and NSE values
 755 generally above 0.5.

756



757

758 *Figure B1. Hydrological skill of EFAS at the calibration locations. Colour coding denotes the*
 759 *quality of the KGE during calibration (left half of square) and validation (right half of the square).*
 760 *Adapted from Arnal et al. (2019).*

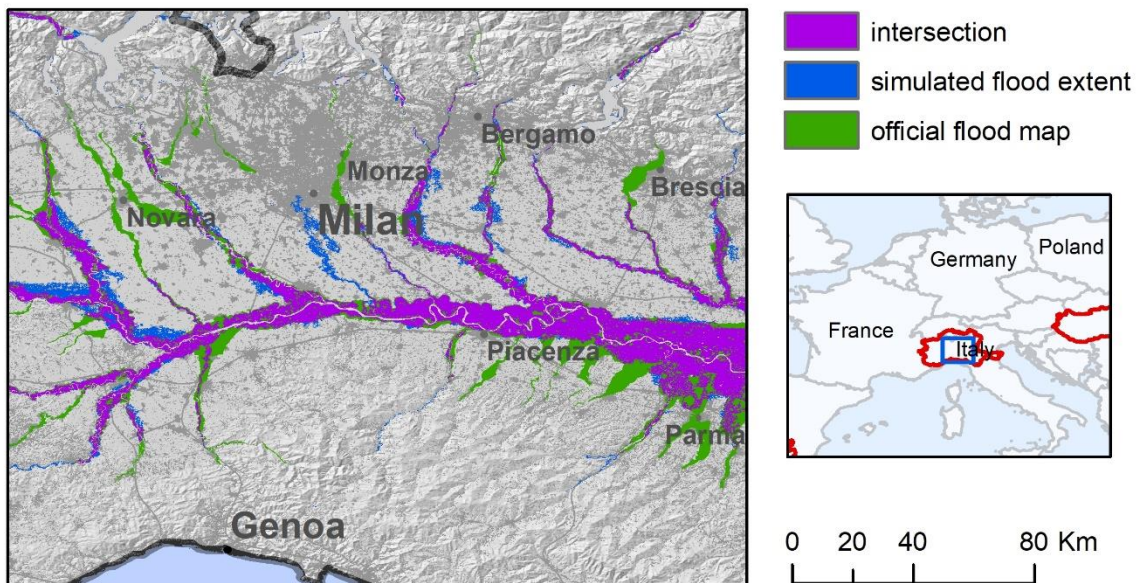
761

762

763 *Appendix C: Additional results*

764 *C1: validation results for the Po River Basin*

765 According to Table 3, the modelled flood maps provide a better reproduction of reference maps
766 for the Po River, compared to other study areas. False alarms are low, while hit ratio (HR) values
767 indicate that two out of every three pixels in the reference map are correctly identified as flooded.
768 The analysis of reference and modelled maps (Figure C1), suggests that the underestimation is
769 partly caused by flooded areas along some tributaries which are not included in modelled maps.
770 Other areas with omission errors are located near confluences of the Po main stem and the major
771 tributaries in Emilia-Romagna, which may depend on the underestimation of peak flow on
772 tributaries. In fact, the results of the LISFLOOD calibration in Figure B1 show better hydrological
773 skill along the Po main stem, compared to some tributaries. Finally, it is likely that the inclusion
774 of smaller tributaries of the river network in the modelled maps would improve the overall
775 performance.
776



777
778 *Figure C1. Comparison of modelled (blue) and reference (green) flood hazard maps (1-in-500-*
779 *year) over the Po river basin, Italy. Purple areas denotes the intersection (agreement) between*
780 *the two set of maps.*

781

782 *C2: validation results for Norway*

783 The results of the modelled flood maps in Norway show a general tendency to overestimate flood
784 extent for the 1-in-100-year events, with high values for both hit ratio (HR) and false alarm ratio
785 (FAR). Such a result is in fact largely influenced by the relatively small extent and discontinuous
786 coverage of reference maps. Flood-prone areas for the 1-in-100-year official maps only cover 215
787 km², possibly due to the low density of populated places in Norway, while they cover between
788 4700 and 5700 km² for England, Spain and Hungary. As for Spain, we applied a 5km buffer to
789 restrict the area of comparison around reference maps, yet this leads to spurious overestimation
790 around the edges of reference map polygons. Notably, the performance improves markedly with
791 the use of a 1km buffer as in Wing et al., (2017), which results in increased critical success index
792 (CSI) scores up to nearly 0.50.

793 The results of reported by Arnal et al. (2019) and summarized in Figure B1 suggest an acceptable
794 hydrological skill of the LISFLOOD calibration in Norway, with a majority of gauge stations
795 scoring KGE values above 0.5. In the areas with lower scores, the model performance for low-
796 probability flood events might be influenced by an incorrect estimation of peak discharges driven
797 by snow melt, which plays a relevant role in determining low-probability flood events.

798

799 *C3: Influence of correcting elevation data with land use*

800 We tested the results of correcting CCM DEM elevation data with vegetation cover in
801 Scandinavia, where the percentage of land covered by forests is more relevant than in the other
802 regions included in the modelled flood maps. For the 1-in100-year flood maps, the overall
803 difference in flood extent between the corrected and uncorrected maps is less than 4%, and similar
804 values were found for the other return periods. Moreover, the HR, FAR and CSI values of two
805 set of maps differ by less than 2% when calculated against the 1-in100-year official map in
806 Norway, probably because forested areas have not been considered as relevant flood-prone areas.
807 These results suggest that the simulation of densely vegetated areas have a limited importance in
808 determining the overall performance of modelled flood maps in Europe.

809

810

811 *Author contribution*

812

813 FD: conceptualization, formal analysis, investigation, data curation writing (original draft, review
814 and editing); LA: methodology, investigation, writing (review and editing); AB: data curation,
815 validation, visualization; JS: investigation, writing (review and editing); PS: conceptualization,
816 project administration, writing (original draft, review and editing)

817

818 *Competing interests*

819 The authors declare that they have no conflict of interest.

820

821 *Acknowledgements*

822 This study has been partially funded by the COPERNICUS programme and by an administrative
823 arrangement with Directorate General 'European Civil Protection and Humanitarian Aid
824 Operations (DG ECHO) of the European Commission. EFAS is operated and financed as part of
825 the Copernicus Emergency Management Service. The authors would like to thank Niall
826 McCormick for his valuable suggestions on the early versions of the manuscript

827

828

829 *References*

- 830 Alfieri, L., Salamon, P., Bianchi, A., Neal, J., Bates, P.D., Feyen, L., 2014. Advances in pan-
831 European flood hazard mapping, *Hydrol. Process.*,28 (18), 4928-4937, doi:10.1002/hyp.9947.
- 832 Alfieri L., Feyen L., Dottori F., Bianchi A., 2015. Ensemble flood risk assessment in Europe
833 under high end climate scenarios. *Global Environmental Change* 35, 199–212.
- 834 Alfieri, L., L. Feyen, and G. D. Baldassarre (2016), Increasing flood risk under climate
835 change: a pan-European assessment of the benefits of four adaptation strategies, *Clim. Change*,
836 136(3), 507–521, doi:10.1007/s10584-016-1641-1.
- 837 Arnal, L., S.-S. Asp, C. Baugh, A. de Roo, J. Disperati, F. Dottori, R. Garcia, M.
838 GarciaPadilla, E. Gelati, G. Gomes, M. Kalas, B. Krzeminski, M. Latini, V. Lorini, C. Mazzetti,
839 M. Mikulickova, D. Muraro, C. Prudhomme, A. Rauthe-Schöch, K. Rehfeldt, P. Salamon, C.
840 Schweim, J.O. Skoien, P. Smith, E. Sprokkereef, V. Thiemig, F. Wetterhall, M. Ziese, 2019.
841 EFAS upgrade for the extended model domain – technical documentation, EUR 29323 EN,
842 Publications Office of the European Union, Luxembourg, 2019, ISBN 978-92- 79-92881-9, doi:
843 10.2760/806324, JRC111610.
- 844 Autorita` di bacino del fiume Po (AdB Po): Progetto di Variante al PAI: mappe della
845 pericolosita` e del rischio di alluvione (in Italian), [https://pianoalluvioni.adbpo.it/progetto-](https://pianoalluvioni.adbpo.it/progetto-esecutivodelleattivita/)
846 [esecutivodelleattivita/](https://pianoalluvioni.adbpo.it/progetto-esecutivodelleattivita/), accessed on 2020-04-03, 2012.
- 847 Bates, P. D., De Roo, A. P. J., 2000. A simple raster-based model for flood inundation
848 simulation, *J. Hydrol.*, 236 (1–2), 54–77.
- 849 Bates P.D., Horritt M.S., and Fewtrell T.J., 2010. A simple inertial formulation of the shallow
850 water equations for efficient two-dimensional flood inundation modelling. *Journal of Hydrology*,
851 387, 33-45.
- 852 Bates, P. D., Quinn, N., Sampson, C., Smith, A., Wing, O., Sosa, J., et al. (2021). Combined
853 modeling of US fluvial, pluvial, and coastal flood hazard under current and future climates. *Water*
854 *Resources Research*, 57, e2020WR028673. <https://doi.org/10.1029/2020WR028673>
- 855 Baugh, C. A., Bates, P. D., Schumann G., Trigg, M.A., 2013. SRTM vegetation removal and
856 hydrodynamic modeling accuracy, *Water Resour. Res.* 49, 5276–5289, doi:10.1002/wrcr.20412.
- 857 Barredo JI, de Roo A, Lavalle C. 2007. Flood risk mapping at European scale. *Water Science*
858 *and Technology* 56: 11–17.

859 Bontemps, S., et al., 2009. GLOBCOVER -Products description and validation report, Univ.
860 Catholique de Louvain.

861 Burek, P., Knijff van der, J., Roo de, A., 2013. LISFLOOD, Distributed Water Balance and
862 Flood Simulation Model Revised User Manual 2013. Publications Office, Luxembourg.

863 Copernicus Land Monitoring Service. Corine Land Cover. [http://land.copernicus.eu/pan-](http://land.copernicus.eu/pan-european/corine-land-cover)
864 [european/corine-land-cover](http://land.copernicus.eu/pan-european/corine-land-cover) (accessed on 12/2/2020).

865 Dottori, F., Alfieri, L., Salamon, P., Bianchi, A., Feyen, L., Lorini, V., 2016a: Flood hazard
866 map for Europe - 100-year return period. European Commission, Joint Research Centre (JRC)
867 [Dataset] PID: http://data.europa.eu/89h/jrc-floods-floodmapeu_rp100y-tif

868 Dottori, F., Salamon, P., Bianchi, A., Alfieri, L., Hirpa, F.A., Feyen, L., 2016b. Development
869 and evaluation of a framework for global flood hazard mapping. *Advances in Water Resources*
870 94, 87–102.

871 Dottori F., Kalas M., Salamon P., Bianchi A., Alfieri, L., Feyen L., 2017. An operational
872 procedure for rapid flood risk assessment in Europe. *Nat. Hazards Earth Syst. Sci.*, 17, 1111-
873 1126, <https://doi.org/10.5194/nhess-17-1111-2017>.

874 Dottori, F., Szewczyk, W., Ciscar, J.C., Zhao, F., Alfieri, L., Hirabayashi, Y., Bianchi, A.,
875 Frieler, K., Betts, R.A., Feyen, L., 2018 Increased human and economic losses from river floods
876 with anthropogenic warming. *Nature Climate Change*, 8(9), 781-786,
877 <https://doi.org/10.1038/s41558-018-0257-z>

878 Dottori F., Bianchi A., Alfieri, L., Skoien, J., Salamon P., 2020a. River flood hazard maps for
879 Europe and the Mediterranean Basin region. JRC Data Catalogue, accessible at
880 <https://data.jrc.ec.europa.eu/dataset/1d128b6c-a4ee-4858-9e34-6210707f3c81> .

881 Dottori F, Mentaschi L, Bianchi A, Alfieri L and Feyen L, 2020b. Adapting to rising river
882 flood risk in the EU under climate change, EUR 29955 EN, Publications Office of the European
883 Union, Luxembourg, 2020, ISBN 978-92-76-12946-2 , doi:10.2760/14505, JRC118425.

884 European Commission (EC), 2007. Directive 2007/60/EC of the European Parliament
885 and of the Council on the assessment and management of flood risks, Official Journal
886 of the European Communities, Brussels, available at: [http://eur-lex.europa.eu/legal-](http://eur-lex.europa.eu/legal-content/EN/TXT/?uri=CELEX%3A32007L0060)
887 [content/EN/TXT/?uri=CELEX%3A32007L0060](http://eur-lex.europa.eu/legal-content/EN/TXT/?uri=CELEX%3A32007L0060) (accessed on 13/5/2020).

888 ESA-Airbus, 2019. Copernicus Digital Elevation Model Validation Report, accessed on
889 14/5/2020 at <https://spacedata.copernicus.eu/documents/12833/20611/GEO1988->
890 [CopernicusDEM-RP-001_ValidationReport_V1.0/9bc5d392-c5f2-4118-bd60-db9a6ea4a587](https://spacedata.copernicus.eu/documents/12833/20611/GEO1988-CopernicusDEM-RP-001_ValidationReport_V1.0/9bc5d392-c5f2-4118-bd60-db9a6ea4a587)

891 Feyen L, Dankers R, Bódis K, Salamon P, Barredo JI. 2012. Fluvial floodrisk in Europe in
892 present and future climates. *Climatic Change*: 112(1): 47–62, doi:10.1007/s10584-011-0339-7.

893 Fleischmann A., R. Paiva, W. Collischonn, 2019. Can regional to continental river
894 hydrodynamic models be locally relevant? A cross-scale comparison. *Journal of Hydrology X*,
895 2019.

896 Gupta, H.V., H. Kling, K.K. Yilmaz, G.F. Martinez, 2009: Decomposition of the mean
897 squared error and NSE performance criteria: implications for improving hydrological modelling.
898 *Journal of Hydrology*, 377, 80-91.

899 Hirpa, F.A.; Salamon, P.; Beck, H.E.; Lorini, V.; Alfieri, L.; Zsoter, E.; Dadson, S.J. , 2018.
900 Calibration of the Global Flood Awareness System (GloFAS) using daily streamflow data. *J.*
901 *Hydrol.*, 566, 595–606.

902 Jongman, B., Hochrainer-Stigler, S., Feyen, L., Aerts, J.C.J.H., Mechler, R., Botzen, W.J.W.,
903 Bouwer, L.M., Pflug, G., Rojas, R., Ward, P.J., 2014. Increasing stress on disaster-risk finance
904 due to large floods. *Nat. Clim. Change* 4, 264-268, doi:<http://dx.doi.org/10.1038/nclimate2124>.

905 Knoben, W. J. M., Freer, J. E., and Woods, R. A.: Technical note: Inherent benchmark or not?
906 Comparing Nash–Sutcliffe and Kling–Gupta efficiency scores, *Hydrol. Earth Syst. Sci.*, 23,
907 4323–4331, <https://doi.org/10.5194/hess-23-4323-2019>, 2019.

908 Krause, P., Boyle, D. P., Bäse, F. Comparison of different efficiency criteria for hydrological
909 model assessment. *Advances in Geosciences*, European Geosciences Union, 2005, 5, pp.89-97.

910 Kulp, S.A.; Strauss, B.H. CoastalDEM: A global coastal digital elevation model improved from
911 SRTM using a neural network. *Remote Sens. Environ.* 2018, 206, 231–239.

912 Liu, Y., Bates, P.D., Neal, J.C. and Yamazaki, D., 2019, December. Bare-earth DEM
913 Generation in Urban Areas Based on a Machine Learning Method. In *AGU Fall Meeting*
914 *Abstracts* (Vol. 2019, pp. H41N-1899).

915 Meadows, M.;Wilson, M. A Comparison of Machine Learning Approaches to Improve Free
916 Topography Data for Flood Modelling. *Remote Sens.* 2021, 13, 275.
917 <https://doi.org/10.3390/rs13020275>

918 Ministerio de Medio Ambiente y Medio Rural y Marino (MITECO), 2011. Guía
919 Metodologica para el desarrollo del sistema nacional de cartografía de zonas inundables.
920 Accessed on 18/5/2020 at [https://www.miteco.gob.es/es/agua/temas/gestion-de-los-riesgos-de-](https://www.miteco.gob.es/es/agua/temas/gestion-de-los-riesgos-de-inundacion/snczi/Guia-metodologica-determinacion-zonas-inundables/default.aspx)
921 [inundacion/snczi/Guia-metodologica-determinacion-zonas-inundables/default.aspx](https://www.miteco.gob.es/es/agua/temas/gestion-de-los-riesgos-de-inundacion/snczi/Guia-metodologica-determinacion-zonas-inundables/default.aspx) (in Spanish).
922 Nash, J. E. and Sutcliffe, J. V.: River flow forecasting through conceptual models part I – A
923 discussion of principles, *J. Hydrol.*, 10, 282–290, [https://doi.org/10.1016/0022-1694\(70\)90255-](https://doi.org/10.1016/0022-1694(70)90255-6)
924 6, 1970.

925 The Norwegian Water Resources and Energy Directorate, 2020. Flood Zone Maps. Accessed
926 on 24/4/2020 at <https://www.nve.no/flaum-og-skred/kartlegging/flaum/> (in Norwegian)

927 Paprotny, D., Morales-Nápoles, O., and Jonkman, S. N.: Efficient pan-European river flood
928 hazard modelling through a combination of statistical and physical models, *Nat. Hazards Earth*
929 *Syst. Sci.*, 17, 1267-1283, <https://doi.org/10.5194/nhess-17-1267-2017>, 2017.

930 Sampson, C. C., Smith, A. M., Bates, P. D., Neal, J. C., Alfieri, L., & Freer, J. E. (2015). A
931 high-resolution global flood hazard model. *Water Resources Research*, 51(9), 7358-7381.

932 Scussolini, P., Aerts, J. C. J. H., Jongman, B., Bouwer L. M., Winsemius H. C., de Moel H.,
933 and Ward, P. J., 2015. FLOPROS: an evolving global database of flood protection standards. *Nat.*
934 *Hazards Earth Syst. Sci. Discuss.*, 3, 7275–7309, 2015, doi:10.5194/nhessd-3-7275-2015.

935 Shaw, J., Kesserwani, G., Neal, J., Bates, P., and Sharifian, M. K.: LISFLOOD-FP 8.0: the
936 new discontinuous Galerkin shallow-water solver for multi-core CPUs and GPUs, *Geosci. Model*
937 *Dev.*, 14, 3577–3602, <https://doi.org/10.5194/gmd-14-3577-2021>, 2021.

938 Thielen J., Bartholmes J., Ramos M.H., and De Roo A. (2009). The European flood alert
939 system - part 1: concept and development. *Hydrol. Earth Syst. Sci.* 13, 125-140.

940 Trigg, M. et al., 2016. The credibility challenge for global fluvial flood risk analysis. *Environ.*
941 *Res. Lett.* 11 094014

942 United Nations Office for Disaster Risk Reduction (UNISDR), 2015. Sendai Framework for
943 Disaster Risk Reduction 2015–2030 (www.unisdr.org/we/inform/publications/43291)

944 Van der Knijff, J.M., Younis, J., de Roo, A.P.J., 2010. LISFLOOD: a GIS-based
945 distributed model for river basin scale water balance and flood simulation. *Int. J. Geogr. Inf. Sci.*
946 24, 189-212.

947 Vogt et al., 2007. A pan-European river and catchment database, JRC Reference Reports,
948 doi:0.2788/35907.

949 Ward, P.J. et al., 2015. Usefulness and limitations of global flood risk models. *Nature Climate*
950 *Change* 5, 712–715.

951 Wendi, D.; Liang, S.-Y.; Sun, Y.; Doan, C.D. An innovative approach to improve SRTM
952 DEM using multispectral imagery and artificial neural network. *J. Adv. Model. Earth Syst.* 2016,
953 8, 691–702.

954 Wing, O. E., Bates, P. D., Sampson, C. C., Smith, A. M., Johnson, K. A., & Erickson, T. A.
955 (2017). Validation of a 30 m resolution flood hazard model of the conterminous United States.
956 *Water Resources Research*, 53(9), 7968-7986, doi:10.1002/2017WR020917.

957 Wing, O. E. J., Sampson, C. Bates, P. D., Quinn, N., Smith, A. M., Neal, J. C., C. (2019a). A
958 flood inundation forecast of Hurricane Harvey using a continental-scale 2D hydrodynamic model.
959 *Journal of Hydrology* X 4 , 100039.

960 Wing, O. E. J., Bates, P. D., Neal, J. C., Sampson, C. C., Smith, A. M., Quinn, N., et al.
961 (2019b). A New Automated Method for Improved Flood Defense Representation in Large-Scale
962 Hydraulic Models. *Water Resources Research* 55, 11007-11034, <https://doi.org/2019WR025957>

963 Yamazaki, D., Ikeshima, D., Tawatari, R., Yamaguchi, T., O'Loughlin, F., Neal, J., Sampson,
964 C., Kanae, S., Bates, P. D. (2017). A high accuracy map of global terrain elevations. *Geophysical*
965 *Research Letters*.

966 Yamazaki, D., Ikeshima, D., Sosa, J., Bates, P. D., Allen, G. H., & Pavelsky, T. M. (2019).
967 MERIT Hydro: a high-resolution global hydrography map based on latest topography dataset.
968 *Water Resources Research*, 55, 5053–5073. <https://doi.org/10.1029/2019WR024873>

969 Zuzanna Zajac, Z., Zambrano-Bigiarini, M., Salamon, P., Burek, P., Gentile, A., Bianchi, A.,
970 2013. Calibration of the LISFLOOD hydrological model for Europe. JRC technical report
971 JRC87717.